ADVANCES IN ATMOSPHERIC SCIENCES, VOL. 36, FEBRUARY 2019, 133–142

• **Original Paper** •

Impact of the Horizontal Heat Flux in the Mixed Layer on an Extreme Heat Event in North China: A Case Study

Ying NA[1,2], Riyu LU[*1,2], Bing LU[3], Min CHEN[3], and Shiguang MIAO[3]

[1]*State Key Laboratory of Numerical Modeling for Atmospheric Sciences and Geophysical Fluid Dynamics, Institute of Atmospheric Physics, Chinese Academy of Sciences, Beijing* 100029*, China*

[2]*College of Earth and Planetary Sciences, University of the Chinese Academy of Sciences, Beijing* 100049*, China*

[3]*Institute of Urban Meteorology, China Meteorological Administration, Beijing* 100089*, China*

(Received 22 June 2018; revised 12 September 2018; accepted 10 October 2018)

ABSTRACT

Extreme heat over the North China Plain is typically induced by anomalous descending flows associated with anticyclonic circulation anomalies. However, an extreme heat event that happened in the North China Plain region on 12–13 July 2015, with maximum temperature higher than 40°C at some stations, was characterized by only a weak simultaneous appearance of an anomalous anticyclone and descending flow, suggesting that some other factor(s) may have induced this heat event. In this study, we used the forecast data produced by the Beijing Rapid Updated Cycling operational forecast system, which predicted the heat event well, to investigate the formation mechanism of this extreme heat event. We calculated the cumulative heat in the mixed-layer air column of North China to represent the change in surface air temperature. The cumulative heat was composed of sensible heat flux from the ground surface and the horizontal heat flux convergence. The results indicated that the horizontal heat flux in the mixed layer played a crucial role in the temporal and spatial distribution of high temperatures. The horizontal heat flux was found to be induced by distinct distributions of air temperatures and horizontal winds at low levels during the two days, implying a complexity of the low-level atmosphere in causing the extreme heat.

Key words: extreme heat, North China Plain, horizontal heat flux, sensible heat flux, warm advection

Citation: Na, Y., R. Y. Lu, B. Lu, M. Chen, and S. G. Miao, 2019: Impact of the horizontal heat flux in the mixed layer on an extreme heat event in North China: A case study. *Adv. Atmos. Sci.*, **36**(2), 133–142, https://doi.org/10.1007/s00376-018-8133-3.

1. Introduction

The North China Plain (NCP) is one of the three largest plains in China. It is also one of most highly populated areas in China, as well as in the world, with about 250 million of people living in the region. In addition, the NCP is an important base for grain production, with about one-fifth of the country's grain production coming from this region. The climate of the NCP is a typical continental monsoon climate, characterized by hot summers and cold winters. Heat waves pose a significant threat to human health, agriculture, and the supply of water and electricity in the region, especially against the background of global warming. In fact, the number of extreme high temperature days in North China presents an increasing trend since 1960 and has a remarkable peak in the late 1990s (Zhang et al., 2004; Zhang et al., 2006; Wei and Sun, 2007; Wei and Chen, 2009; Ding and Qian, 2011); plus, the spatial extent affected by heat waves has also increased since 1960 (Li et al., 2017). Therefore, it is urgent to better understand and more precisely forecast heat wave events in the NCP region.

Large-scale circulations are widely used to explain the occurrence of heat wave events, and are thus considered as a crucial factor in accurately forecasting the weather of heat wave events. Although various patterns of large-scale circulations can cause heat waves (Harpaz et al., 2014; Chen and Lu, 2015, 2016), anticyclonic circulations are the most typical patterns for heat waves in China (Chen et al., 2016; Gao et al., 2017; Wang et al., 2017; Chen et al., 2018), as well as worldwide (Loikith and Broccoli, 2012; Grotjahn et al., 2016). For the NCP, the North China high is the most well-known type of large-scale circulation responsible for the occurrence of heat waves (Zhang et al., 2004; Qian et al., 2005; Chen and Lu, 2015). The North China high is characterized by an anticyclone in the lower troposphere and a ridge in the middle and upper troposphere, and generally moves from Northwest China to North China (Qian et al., 2005; Zheng and Wang, 2005; Lian et al., 2008). Descending flows are associated with the North China High, causing adiabatic heating and re-

* Corresponding author: Riyu LU
Email: lr@mail.iap.ac.cn

sultant high surface temperatures (Zheng and Wang, 2005; Lian et al., 2008). In addition, an anomalously northwest extension of the western North Pacific subtropical high also contributes to extreme heat events in North China (Wei et al., 2004; Zhang et al., 2004; Wei and Sun, 2007).

In this study, however, we report a heat wave event that was strong but featured neither an apparent North China high nor a northwestward-extended western North Pacific subtropical high. This extreme heat event happened in North China on 12–13 July 2015. The temperature increased rapidly on 12 July and reached a peak on 13 July. The observed highest daily maximum temperatures were 38.9°C on 12 July at Miyun station and 41.6°C on 13 July at Anyang station. Despite this event's unusual nature, the Beijing Rapid Updated Cycling (BJ-RUCv2.0) system, which is an operational forecasting system run by the Beijing Meteorological Service since 2008, produced an accurate forecast of it. Therefore, this case provides a good opportunity for us to study, using the forecast results of the BJ-RUCv2.0 system, the formation mechanism of a heat event that cannot otherwise be explained well by the large-scale circulation background.

The rest of this paper is organized as follows: The data and methods are described in section 2. Observational features and forecast results are presented in sections 3 and 4, respectively. Section 5 discusses the possible mechanisms responsible for the occurrence of this event through heat budget analysis. Finally, section 6 summarizes the results.

2. Data and methods

2.1. *Data*

Observed daily mean, maximum and minimum air temperature records at 95 stations in North China in July 2015 were obtained from the National Meteorological Information Center, China Meteorological Administration. In addition, the 3-h temperature data produced by the National Oceanic and Atmospheric Administration, were downloaded from https://gis.ncdc.noaa.gov/maps/ncei/cdo/hourly. The daily homogenized temperature series from 1960 to 2013 were provided by Li et al. (2015) and used as the climatology in this study. The large-scale circulation data were from the European Centre for Medium-Range Weather Forecasts interim reanalysis (ERA-Interim), with a horizontal resolution of 0.5° × 0.5° (Dee et al., 2011).

The numerical simulation data were from the BJ-RUCv2.0 system, which is the operational forecasting system of the Beijing Meteorological Service, China Meteorological Administration. The BJ-RUCv2.0 system is based on version 3.3 of the Weather Research and Forecasting (WRF) model and version 3.3 of the WRF model data assimilation system. It has two independent forecast domains: Domain 1 covers a large part of China [roughly (20°–50°N, 80°–130°E)] with a 9 km resolution, and Domain 2 covers North China [roughly (35°–45°N, 105°–125°E)] with a 3 km resolution. The model has 50 vertical sigma levels. Domain 1 performs 72-h forecasts twice per day, at 0000 UTC and 1200 UTC, and the forecast results provide the boundary conditions for Domain 2. Domain 2 performs 24-h forecasts every 3 h from 0000 UTC. Both domains assimilate observational data, including conventional and intensive sounding and surface data, ship and buoy data, aviation routine weather reports, automatic weather station observations in Beijing, and subgrade GPS precipitation data. Domain 2 also assimilates radar data. The physics parameterization schemes include the RRTM longwave and Dudhia shortwave radiation schemes, the ACM2 PBL parameterization, and the Thompson microphysics parameterization. More detailed information on the BJ-RUCv2.0 system can be found in Chen et al. (2011) and Fan et al. (2013). The forecast results of this system have been used in previous studies (Chen et al., 2011; Liu and Chen, 2014; Lu et al., 2017), which showed that it performs well. In this study, we used the forecast results initiated from 1200 UTC (2000 LST) in Domain 2, to guarantee a continuous daytime forecast.

2.2. *Heat budget analysis*

The temperatures of the atmospheric column are determined by the sensible heat from the ground surface, heat advection, net radiation of the atmospheric column, and the diabatic heating caused by water vapor condensation. Here, we just considered the mixed-layer column, since the surface air temperature is closely related to the mixed-layer atmosphere. The mixed layer is defined as the range where the atmosphere is uniformly mixed and the potential temperature vertical gradient is approximately zero. In this event, the potential temperature mixed uniformly below 3 km in the afternoon; therefore, we considered 3 km as the maximum mixed-layer height.

Because there was no precipitation during this extreme event, the diabatic heating related to water vapor condensation could be ignored. Likewise, since the low-level atmospheric column absorbs shortwave radiation and loses longwave radiation in similar amounts, the temperature variation caused by radiation could also be neglected. In addition, because the vertical wind speed in the lower troposphere was weak, the heat exchange caused by vertical advection near the top of the mixed-layer was two orders of magnitude smaller than the sensible heat from ground surface (data not shown). Thus, the entrainment heat could be neglected too.

Therefore, the heat budget equation based on per unit air column in the mixed layer could be expressed as follows—the same as in Takane and Kusaka (2011):

$$Q_{\mathrm{C}} = c_p \rho \int_{Z_{\mathrm{G}}}^{Z_{\mathrm{R}}} (\theta_1 - \theta_0)\mathrm{d}z$$

$$Q_{\mathrm{H}} = \int_{t_0}^{t_1} H\mathrm{d}t$$

$$Q_{\mathrm{CONV}} = Q_{\mathrm{C}} - Q_{\mathrm{H}}$$

Here, Q_{C} is the cumulative heat in the air column, which is closely related to temperatures in the mixed layer and the surface air temperatures; Q_{H} is the time-integrated sensible heat flux from the ground surface; and Q_{CONV} is the cumula-

tive heat flux convergence. In addition, the quantity c_p is the specific heat of the atmosphere [1004 J (kg K)$^{-1}$], and ρ is the dry air density (1.29 kg m^{-3}). θ_0 is the potential temperature at 0500 LST (the time of the lowest temperature in one day) and θ_1 is the potential temperature at respective times. The potential temperature is integrated from the ground surface (Z_G) to the top of the mixed layer (Z_R), which was fixed to 3 km above the surface in this study. H is the sensible heat flux from the ground surface, and is integrated from 0500 LST to respective times. Because of the impact of surface terrain in the lower mixed layer, the calculation of temperature advection in the lateral boundary of the atmospheric column may carry large errors, and so Q_{CONV} was calculated as Q_C minus Q_H.

In this study, we defined three regions to quantitatively measure the evolution of temperature. The NCP was denoted by the region (35°–41°N, 113.5°–119.5°E). Two heat-center areas were denoted by rhombus-shaped regions, without considering the curved surface of the earth: (37.5°N, 114°–115.5°E; 40.5°N, 116.5°–118°E) and (35°N, 113.5°–115°E; 38°N, 116°–117.5°E) for 12 and 13 July, respectively. The heat-center areas were determined by the highest forecast 2-m air temperature (T_{max}) on these days.

3. Observed features

Figure 1 shows the observed T_{max} in North China on 12 and 13 July 2015. On both days, T_{max} was higher than 30°C at most stations in North China, and the relatively low T_{max} at some stations was due to the high altitude of these stations. The T_{max} was higher than 35°C in Beijing, Tianjin and the southern part of Hebei Province on 12 July. The highest T_{max}, up to 39.5°C, appeared at Miyun station in Beijing. On 13 July, the high temperature aggravated, extending southward and covering the entire NCP.

Figure 2 shows the observed T_{max} anomalies relative to the climatological average, which is the T_{max} averaged over 54 years from 1960 to 2013 on 12 and 13 July. Almost all the stations present positive anomalies in North China, including the NCP. The high T_{max} anomalies appear over the northern part of North China on 12 July, and extend southward to the southern part of the NCP on 13 July. The T_{max} anomaly averaged over the NCP was 4.4°C on 12 July and 6.7°C on 13 July. The greatest T_{max} anomaly reached 8.5°C on 12 July at Miyun station and 9.7°C on 13 July at Anyang station.

Figure 3 shows the evolution of T_{max} averaged over the stations on the NCP. The normal T_{max} is about 30°C. During 1 July to 11 July, the T_{max} in 2015 was near to normal and the difference with the climatological mean was less than 2°C. However, during 12–14 July, the T_{max} was much higher than the climatological mean, and the difference reached 6°C on 13 July. The T_{max} decreased on 14 July and became normal again on 15 July.

As mentioned in the introduction, this heat wave event cannot simply be explained by the prevailing subsidence associated with a high-pressure ridge. Figure 4 shows the 500-hPa geopotential height and vertical wind at 1400 LST on 12 and 13 July 2015. The geopotential height was similar on these two days. As highlighted by the black boxes, the NCP was located at the margins of a weak anticyclone, which was accompanied by two cyclones, to the west and to the east. The eastern cyclone was a tropical depression downgraded from Typhoon Chan-hom. Corresponding to the anticyclone, there was descending flow in this area. However, the descending flow was very weak, and the 500-hPa vertical wind averaged over the NCP was only 0.09 Pa s^{-1} on 12–13 July. The vertical wind was also weak in the lower troposphere (not shown). Therefore, such strong hot weather cannot be explained well by adiabatic heating caused by descending flow associated with a weak ridge. There must have been other factors involved.

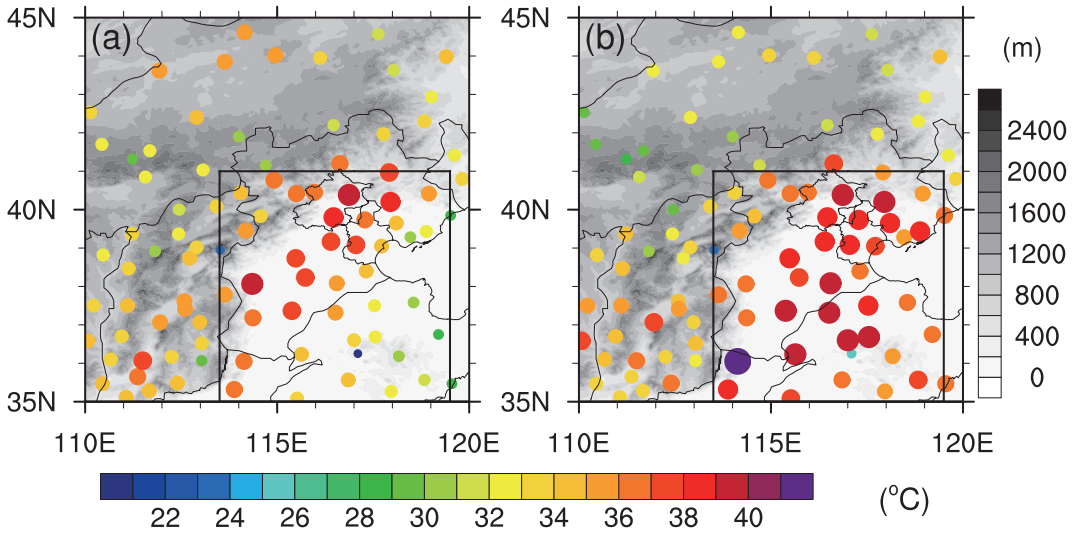

Fig. 1. Observed max 2-m air temperature (color scale; units: °C) in North China on (a) 12 July 2015 and (b) 13 July 2015. The terrain height (units: m) is represented by the grayscale shading. The NCP is highlighted by the square frame.

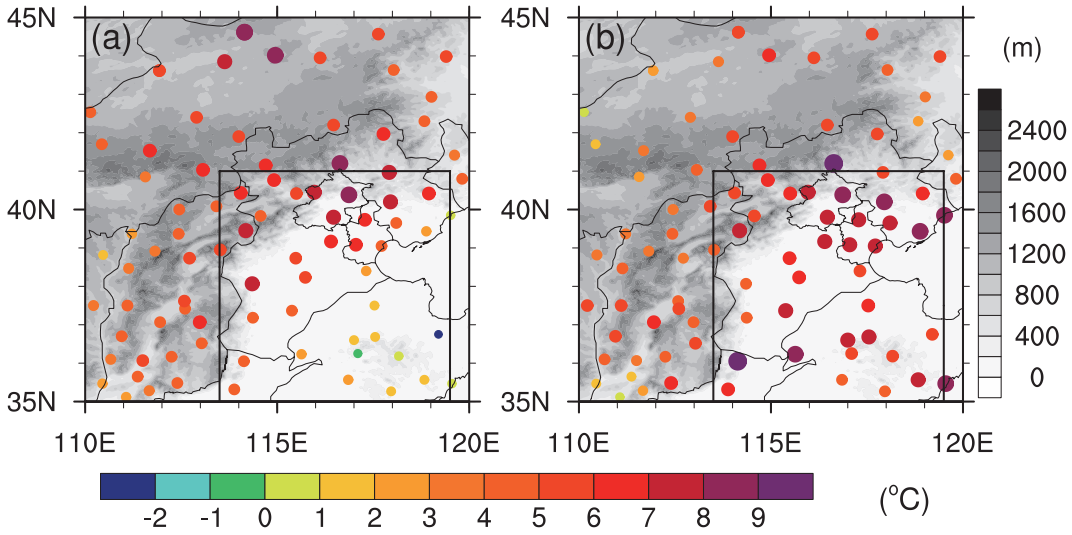

Fig. 2. Observed T_{max} anomalies (color scale; units: °C) relative to the 54-yr climatological average (1960–2013) on (a) 12 July 2015 and (b) 13 July 2015. The terrain height (units: m) is represented by the grayscale shading. The NCP is highlighted by the square frame.

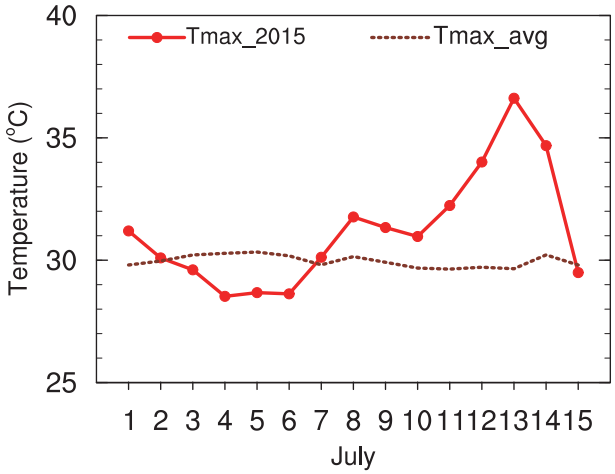

Fig. 3. Time series of T_{max} averaged over stations on the NCP (Tmax_2015), from July 1 to July 15 of 2015 and the climatological average (Tmax_avg), during 1–15 July 2015.

4. Forecast temperatures

Figure 5 shows the observed and forecast surface air temperature from 2000 LST 10 July to 2000 LST 13 July. The observed result is the temperature averaged over the stations on the NCP at intervals of 3 h, and the forecast result is the temperature averaged over the grids of the NCP at intervals of 1 h. The maximum and minimum temperatures increased day by day from 10 to 13 July. The daily maximum and minimum temperatures occurred at approximately 1600 LST and 0500 LST, respectively, both in the observed and forecast data. On 12 July, the temperature ranged from a minimum temperature of 23°C to a maximum temperature of 35°C, and from 24°C to 36°C on 13 July. The forecast temperatures were closely consistent with the observed ones, indicating that this extreme heat event was predicted well.

Figure 6 shows the spatial distribution of the forecast temperature at 1600 LST on these two days. High surface air temperatures appeared over the NCP. In particular, the highest temperatures occurred in Beijing, Tianjin and southern Hebei Province on 12 July; and southern Hebei Province, northern Henan Province and eastern Shandong Province on 13 July. These two regions for highest temperatures on these two days are denoted by the rhombus-shaped regions in Fig. 6, and are defined as heat-center areas. The forecast T_{max} distributions were also in good agreement with the observed ones, shown in Fig. 1. Since BJ-RUCv2.0 predicted both the temporal and spatial distributions of temperatures well, and since the simulation result had various physical quantities and a high resolution, especially in the boundary layer, the forecast data could be used to investigate the underlying mechanism of the extreme heat event, as reported in the next section.

Figure 7 shows a time–height cross section of forecast potential temperatures averaged over the NCP and heat-center areas on 12 and 13 July 2015. The potential temperatures exhibited a clear diurnal cycle below 3 km, but not above this height. Below 3 km, from sunrise to afternoon (from about 0500 LST to 1600 LST), the potential temperatures increased with time rapidly. The potential temperatures were higher in the heat-center areas than in the NCP, and higher on 13 July than on 12 July, as shown by the reference black lines of 312 K. These variations of potential temperature were consistent with the variations of surface air temperature.

5. Heat budget analysis

We integrated the cumulative heat of every unit mixed-layer column in North China from 0500 LST to 1600 LST using the equations in section 2. The spatial distributions are given in Fig. 8. The cumulative heat (Q_C) was positive in the entire NCP on 12 July and in large parts of the NCP on 13 July (Figs. 8a and b), and the positive cumulative heat

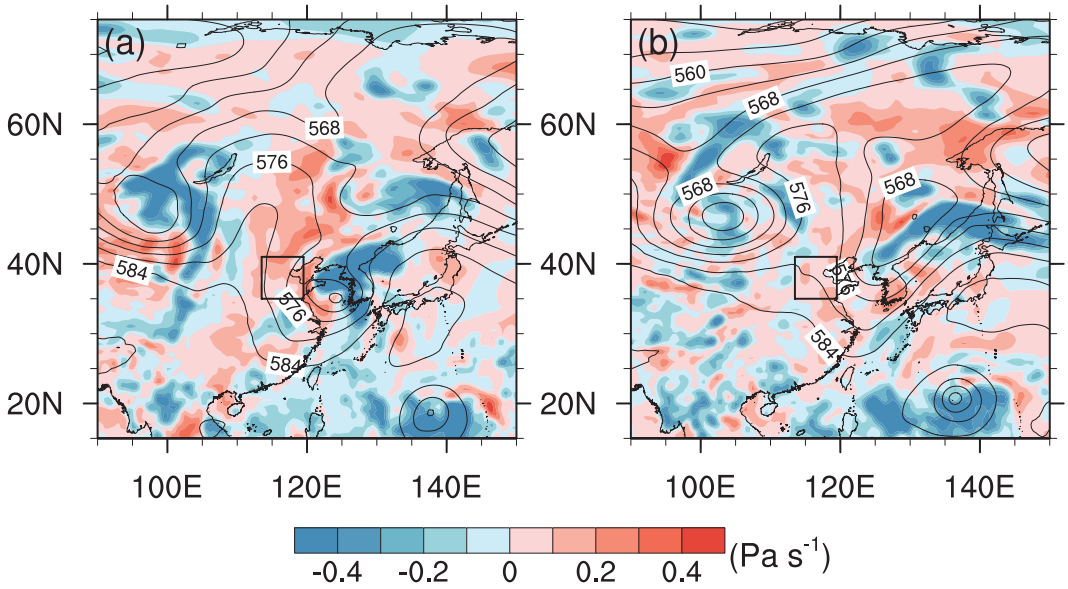

Fig. 4. The 500-hPa geopotential height (contours; units: m) and vertical wind speed (color scale; units: Pa s^{-1}) at 1400 LST on (a) 12 July 2015 and (b) 13 July 2015. The NCP is highlighted by the square frame.

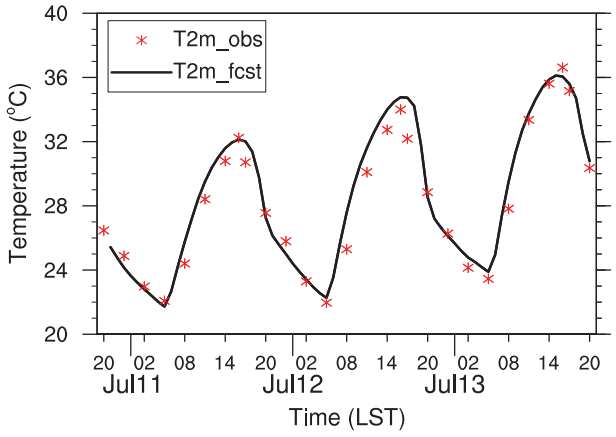

Fig. 5. Observed average temperature of stations on the NCP (T2m_obs), and the forecast average temperature over the NCP (T2m_fcst), from 2000 LST 10 July to 2000 LST 13 July 2015.

indicated an increase in the heat and temperature in the whole air column. The highest values were located in Beijing, Tianjin and southern Hebei Province on 12 July, and shifted to southern Hebei Province, northern Henan Province and eastern Shandong Province on 13 July. The regions of highest values corresponded well to the heat-center areas on these two days. Negative values appeared over Inner Mongolia and extended into the northwest corner of the NCP. The negative values were consistent with the relative decrease in surface air temperature in these regions (Fig. 1). In summary, the cumulative heat could represent the surface air temperature well.

The sensible heat flux (Q_H) was distributed uniformly in North China on both days (Figs. 8c and d). This uniform distribution was unsurprising, as the ground surface accepts solar radiation at similar amounts on clear days and then transports the heat to the air in the mixed layer.

By contrast, the horizontal heat flux convergence (Q_{CONV}) featured an obvious spatial distribution (Figs. 8e and f). This distribution was similar to that of the cumulative heat, which was expected, since the cumulative heat is the sum of the horizontal heat flux convergence and sensible heat flux, and the sensible heat flux showed a uniform distribution. In particular, the horizontal heat flux convergence had higher values in the heat-center areas on both days. In the heat-center areas, vast quantities of heat gathered, resulting in the extremely high temperatures. Based on these results, we can conclude that the horizontal heat flux convergence determined the spatial distribution of the cumulative heat and the resultant southward shift of the heat-center areas.

Figure 9 shows the time series of cumulative heat in the NCP and heat-center areas. In both the NCP and heat-center areas, the cumulative heat increased from early morning to early evening on 12 July, and then reached its peak at around 1600 LST before decreasing slightly thereafter on 13 July. These variations of cumulative heat were closely consistent with those of potential temperature (Fig. 7). For instance, the peak cumulative heat at around 1600 LST 13 July corresponded well to the maximum potential temperature.

Both the sensible heat flux and horizontal heat flux convergence contributed greatly to the cumulative heat increase mentioned above. The sensible heat flux contributed more than the horizontal heat flux convergence in the NCP (Figs. 9a and b). However, in the heat-center areas, the contribution of horizontal heat flux convergence was comparable to that of sensible heat flux on both days (Figs. 9c and d). In addition, the sensible heat flux exhibited similar variation between the NCP and heat centers for both the days, in agreement with its spatially uniform distribution (Figs. 8c and d). By contrast, the horizontal heat flux convergence showed a clear difference between the NCP and heat-center areas, being stronger

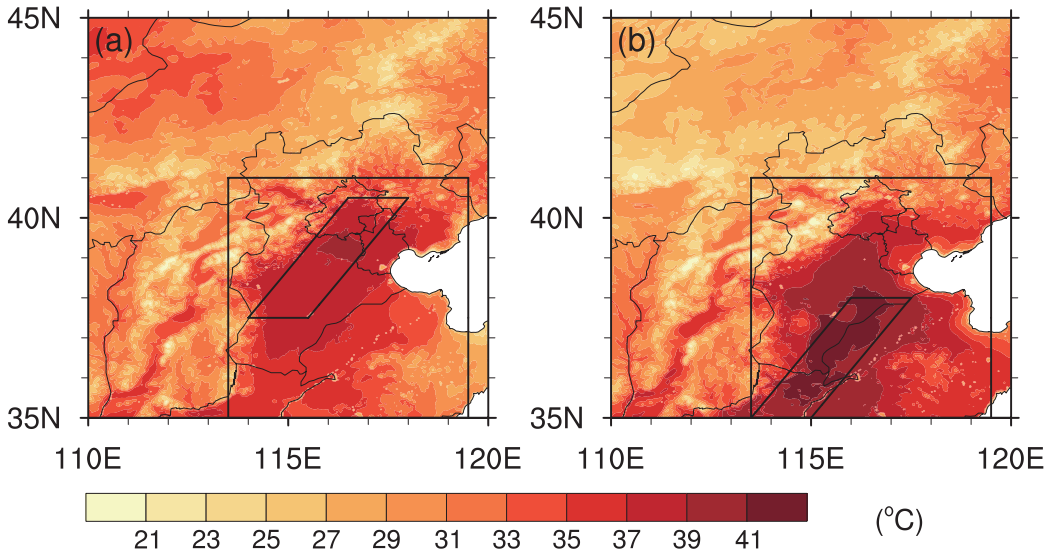

Fig. 6. Forecast 2-m air temperature (color scale; units: °C) at 1600 LST on (a) 12 and (b) 13 July 2015. The NCP is highlighted by the square frame. Heat-center areas are highlighted by the rhombus.

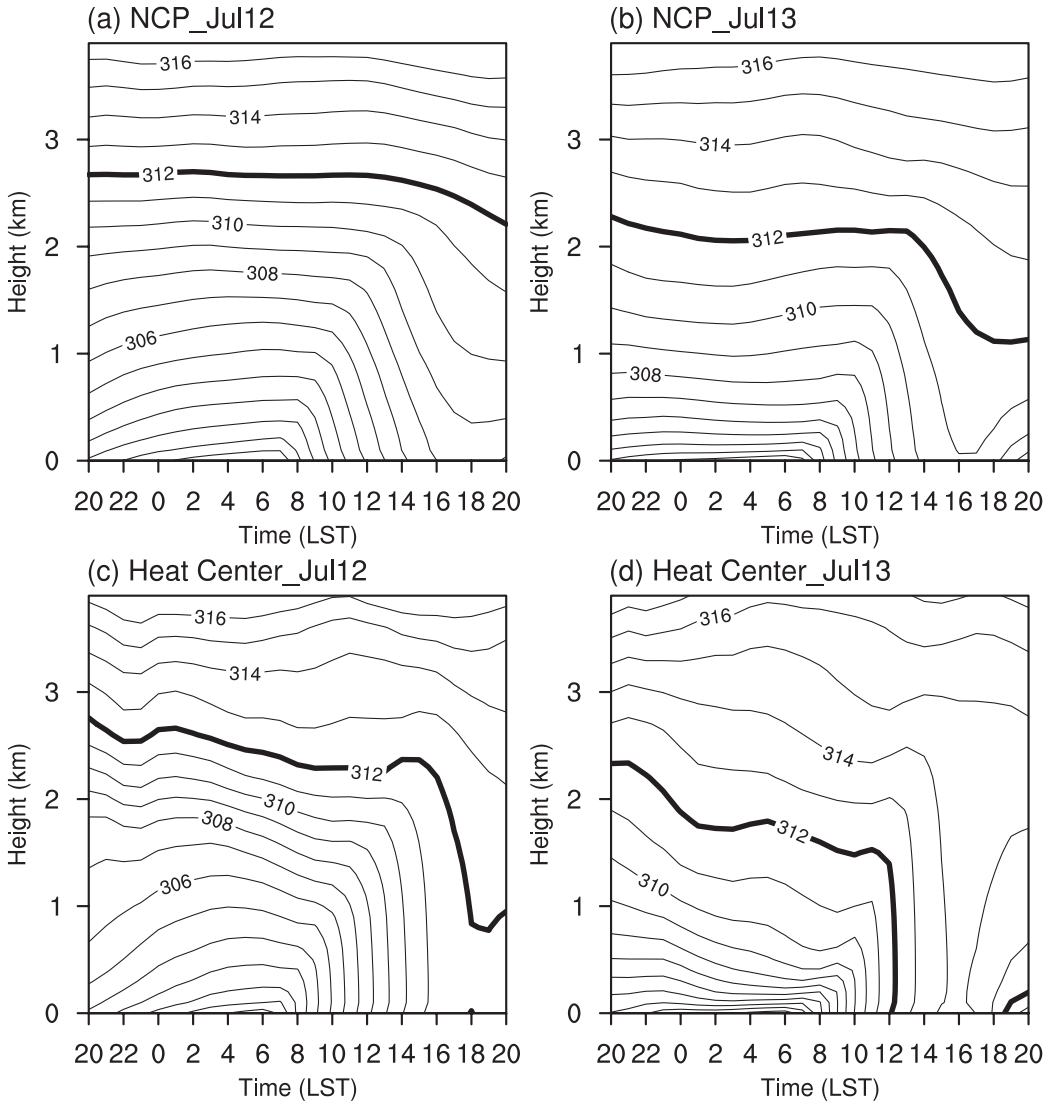

Fig. 7. Time–height cross section of forecast potential temperature (units: K) averaged over the (a, b) NCP and (c, d) heat-center area on (a, c) 12 and (b, d) 13 July 2015.

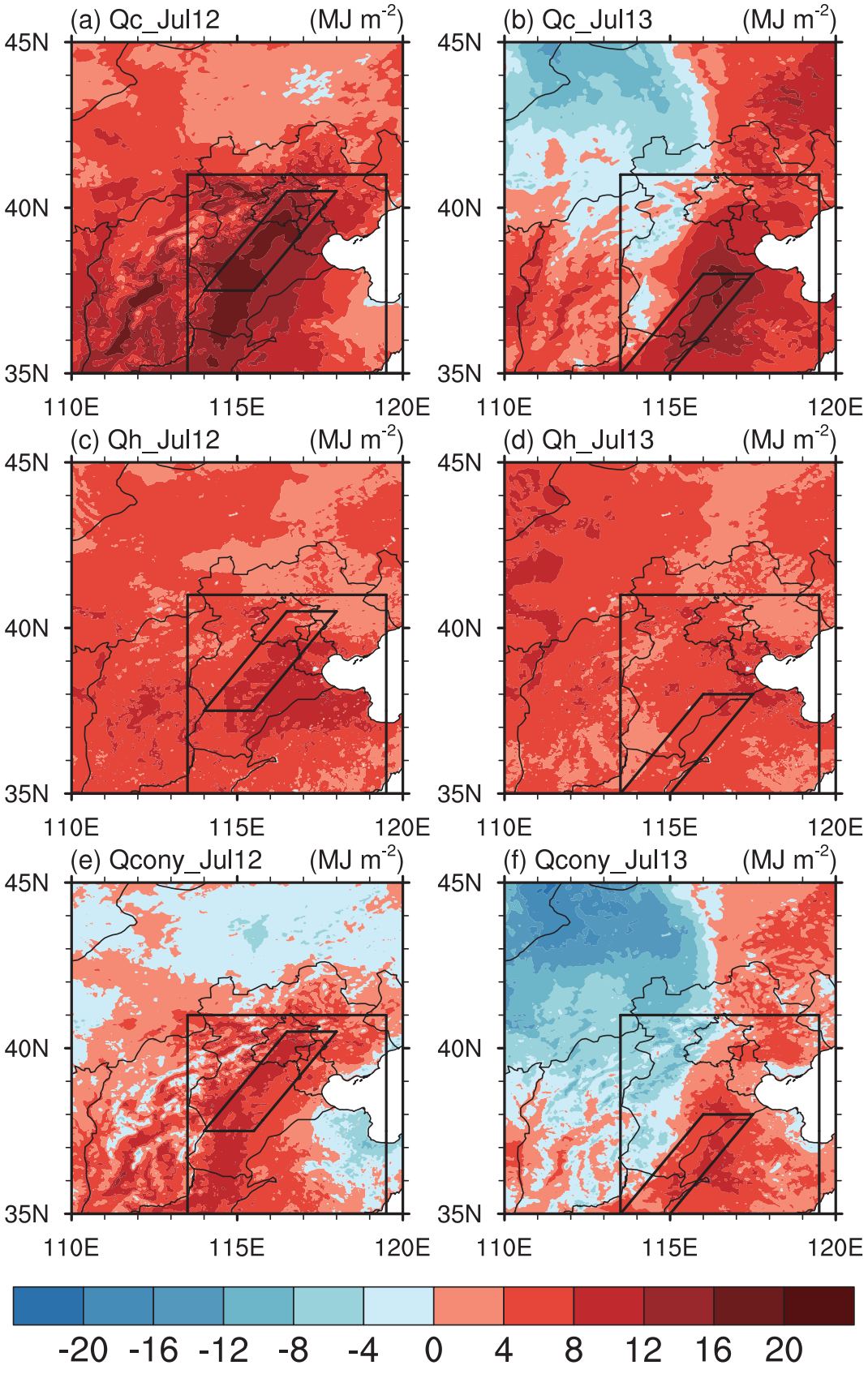

Fig. 8. Integrated cumulative heat (color scale; units: MJ m^{-2}) from 0500 LST to 1600 LST on (a, c, e) 12 and (b, d, f) 13 July 2015: (a, b) cumulative heat (Q_C); (c, d) sensible heat flux (Q_H); (e, f) horizontal heat flux convergence (Q_{CONV}).

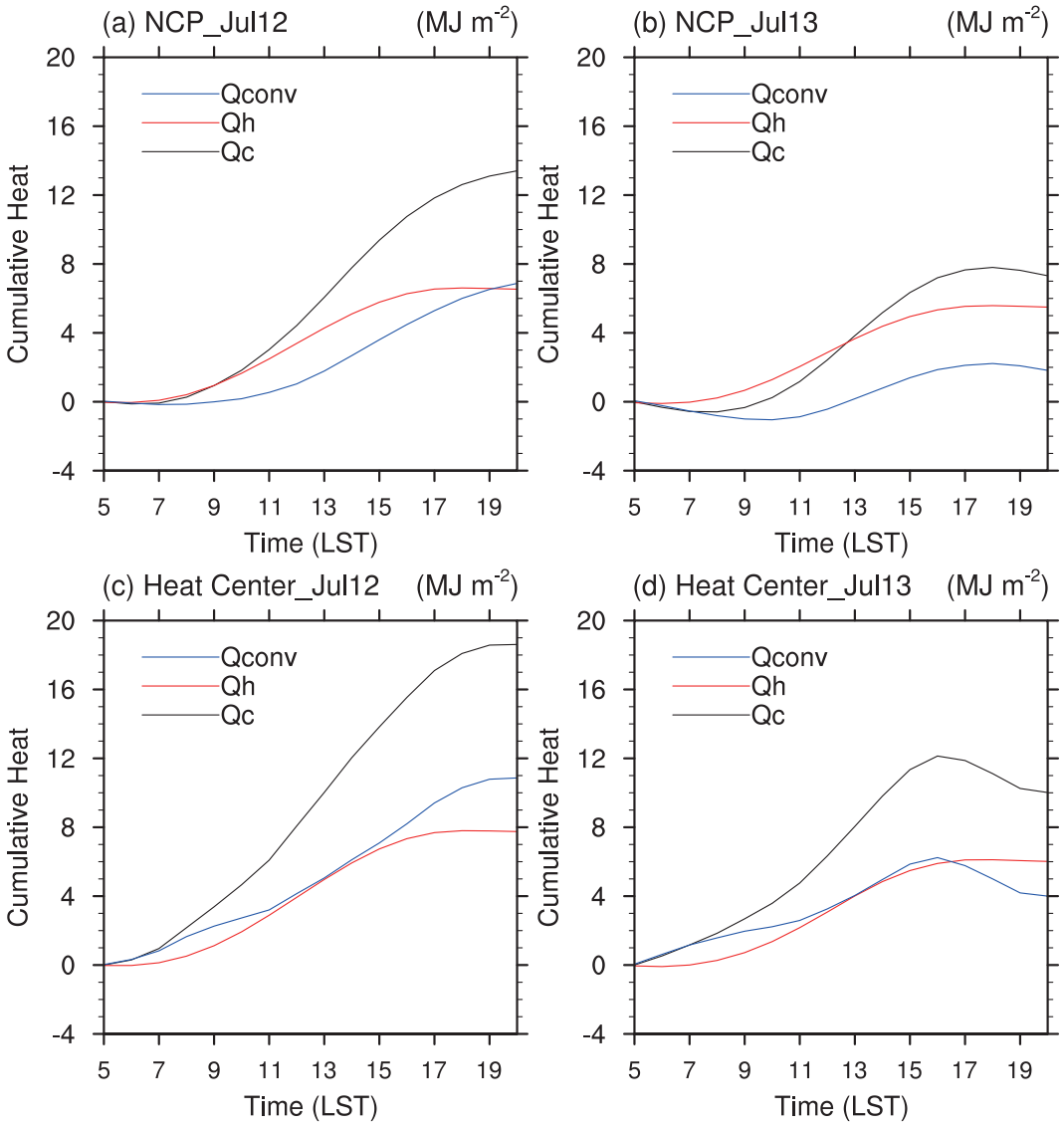

Fig. 9. Time series of cumulative heat (units: MJ m^{-2}) in the (a, b) NCP and (c, d) heat-center areas on (a, c) 12 and (b, d) 13 July 2015.

in the latter. Therefore, the difference in cumulative heat between the NCP and heat-center areas was caused by the horizontal heat flux convergence. These results suggest that the horizontal heat flux convergence contributed significantly to the cumulative heat increase and its spatial distribution.

The horizontal heat flux convergence is determined by the horizontal advection of potential temperature in the mixed layer. Therefore, we examined the air temperatures and horizontal winds at 850 hPa over the NCP (Fig. 10). We also examined these two variables at other levels, such as 800 and 925 hPa, and obtained similar results (data not shown). Therefore, the pressure level of 850 hPa can be used to illustrate the horizontal distributions of temperature and wind in the mixed layer. Since the NCP is located on the eastern lee sides of adjacent mountains (Fig. 1), the data beneath the ground level in mountain areas were ignored. On 12 July, the temperature was high in the northwest of the NCP, and decreased from northwest to southeast. Therefore, the northerlies resulted in warm horizontal advection to the NCP, particularly to the heat center. On the other hand, on 13 July, high temperatures were located in the southwest, and the temperature generally decreased northeastward. Therefore, southwesterlies resulted in warm horizontal advection. Although both the temperature distribution and wind directions were quite different between these two days, they all resulted in warm horizontal advection and favored high temperatures over the NCP and heat centers. This result suggests that diverse circulations in the mixed layer can be responsible for heat waves in the NCP region. It should also be mentioned that the ERA-Interim data produced results (not shown) similar to the forecast results in Fig. 10, suggesting again that the forecast was accurate and that the forecast results could be used to investigate the formation mechanisms of the heat wave event.

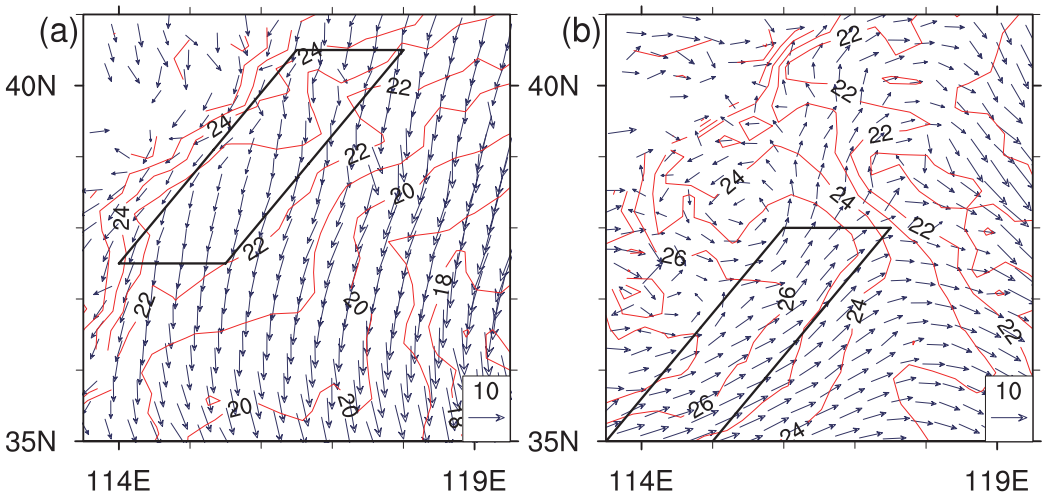

Fig. 10. Forecast air temperatures (contours; units: °C) and horizontal winds (vectors; units: m s^{-1}) at 850 hPa over the NCP at 1400 LST on (a) 12 and (b) 13 July. Heat-center areas are highlighted by the rhombus.

6. Conclusions and discussion

In this study, we quantitatively investigated the formation mechanisms of an extreme heat event that happened in North China on 12–13 July 2015. Daily maximum temperatures higher than 35°C were recorded by most stations in North China, and some were even higher than 41°C. This heat event cannot be explained by the large-scale circulation background. The forecast temperatures from BJ-RUCv2.0 were closely consistent with observation, both in terms of the temporal and spatial distribution. Therefore, we used these forecast data to investigate the underlying mechanism of the extreme heat event.

Analysis of the results indicated that the horizontal heat flux in the lower troposphere played a crucial role in the temporal and spatial distribution of the extreme high temperatures. This was in sharp contrast to typical heat wave events in the NCP region, which are generally induced by adiabatic heating associated with the North China high or westward extension of the western North Pacific subtropical high. Particularly, the horizontal heat flux could explain the spatial distribution of surface air temperatures over the NCP well, which, however, could not be explained by the uniformly distributed sensible heat flux. In addition, the horizontal heat flux was comparable to the sensible heat flux in intensity over the strong heat areas. Finally, we found that the horizontal heat flux was induced by very different patterns of both air temperature and horizontal wind in the mixed layer: northerlies on 12 July and southwesterlies on 13 July, but both bringing warm horizontal advection to the strong heat areas.

In this study, through analysis of an extreme heat event in the NCP region, we have highlighted the role of horizontal heat flux in the mixed layer. This has tended to be neglected by previous studies, which instead emphasize the role of adiabatic heating and solar radiation caused by large-scale circulations in the middle and upper troposphere. The present results suggest that it is necessary for forecast systems to precisely capture the distribution of temperatures and horizontal winds in the lower troposphere as well as the large-scale circulations in the mid-upper troposphere in order to obtain accurate forecasts of heat wave events. Therefore, the interaction between the atmosphere and land will appreciably affect the accuracy of surface air temperature forecasts (Wu et al., 2011; Zhang et al., 2015; Liu et al., 2018; Zhu et al., 2018), and should be adequately taken into account in forecast systems. In addition, the present case study triggers some questions that require further investigation. Can current forecast systems predict heat waves induced by the horizontal heat flux in the mixed layer as accurately as those induced by large-scale circulations? To what extent does the horizontal heat flux contribute to the variability of surface air temperatures, particularly during heat wave events? Does the horizontal heat flux have any special features in other areas, particularly in mountainous and coastal areas? Answering these questions may benefit both weather forecast improvement and a better understanding of regional climate change.

Acknowledgements. This research was sponsored by the Ministry of Science and Technology of China (Grant No. 2015DFA 20870).

REFERENCES

Chen, M., S. Y. Fan, Z. F. Zheng, and J. Q. Zhong, 2011: The Performance of the proximity sounding based on the BJ-RUC system and its preliminary implementation in the convective potential forecast. *Acta Meteorologica Sinica*, **69**(1), 181–194, https://doi.org/10.11676/qxxb2011.016. (in Chinese)

Chen, R. D., and R. Y. Lu, 2015: Comparisons of the circulation anomalies associated with extreme heat in different regions of eastern China. *J. Climate*, **28**(14), 5830–5844, https://doi.org/10.1175/JCLI-D-14-00818.1.

Chen, R. D., and R. Y. Lu, 2016: Role of large-scale circulation and terrain in causing extreme heat in western North China. *J. Climate*, **29**(7), 2511–2527, https://doi.org/10.1175/jcli-d-15-0254.1.

Chen, R. D., Z. P. Wen, and R. Y. Lu, 2016: Evolution of the circulation anomalies and the quasi-biweekly oscillations associated with extreme heat events in southern China. *J. Cli-*

mate, **29**(19), 6909–6921, https://doi.org/10.1175/JCLI-D-16-0160.1.

Chen, R. D., Z. P. Wen, and R. Y. Lu, 2018: Large-scale circulation anomalies and intraseasonal oscillations associated with long-lived extreme heat events in south China. *J. Climate*, **31**(1), 213–232, https://doi.org/10.1175/JCLI-D-17-0232.1.

Dee, D. P., and Coauthors, 2011: The ERA-Interim reanalysis: Configuration and performance of the data assimilation system. *Quart. J. Roy. Meteor. Soc.*, **137**(656), 553–597, https://doi.org/10.1002/qj.828.

Ding, T., and W. H. Qian, 2011: Geographical patterns and temporal variations of regional dry and wet heatwave events in China during 1960–2008. *Adv. Atmos. Sci.*, **28**(2), 322–337, https://doi.org/10.1007/s00376-010-9236-7.

Fan, S. Y., H. L. Wang, M. Chen, and H. Gao, 2013: Study of the data assimilation of radar reflectivity with the WRF 3D-Var. *Acta Meteorologica Sinica*, **71**(3), 527–537, https://doi.org/10.11676/qxxb2013.032. (in Chinese)

Gao, M. N., J. Yang, B. Wang, S. Y. Zhou, D. Y. Gong, and S. J. Kim, 2017: How are heat waves over Yangtze River valley associated with atmospheric quasi-biweekly oscillation? *Climate Dyn.*, 1–17, https://doi.org/10.1007/s00382-017-3526-z. (in Press)

Grotjahn, R., and Coauthors, 2016: North American extreme temperature events and related large scale meteorological patterns: A review of statistical methods, dynamics, modeling, and trends. *Climate Dyn.*, **46**(3–4), 1151–1184, https://doi.org/10.1007/s00382-015-2638-6.

Harpaz, T., B. Ziv, H. Saaroni, and E. Beja, 2014: Extreme summer temperatures in the East Mediterranean-dynamical analysis. *Int. J. Climatol.*, **34**(3), 849–862, https://doi.org/10.1002/joc.3727.

Li, Y., Y. H. Ding, and W. J. Li, 2017: Observed trends in various aspects of compound heat waves across China from 1961 to 2015. *J. Meteor. Res.*, **31**(3), 455–467, https://doi.org/10.1007/s13351-017-6150-2.

Li, Z., Z. W. Yan, and H. Wu, 2015: Updated homogenized Chinese temperature series with physical consistency. *Atmospheric and Oceanic Science Letters*, **8**(1), 17–22, https://doi.org/10.3878/AOSL20140062.

Lian, Z. L., L. S. Gao, Y. C. Zhao, and S. S. Kuang, 2008: Climate characteristic and formation mechanism of continuing high temperature of summer in Shijiazhuang. *Chinese Journal of Agrometeorology*, **29**(4), 387–391, https://doi.org/10.3969/j.issn.1000-6362.2008.04.002. (in Chinese)

Liu, M. J., and M. Chen, 2014: Evaluation of BJ-RUC system for the forecast quality of planetary boundary layer in Beijing Area. *Journal of Applied Meteorological Science*, **25**(2), 212–221, https://doi.org/10.3969/j.issn.1001-7313.2014.02.011. (in Chinese)

Liu, X. J., G. J. Tian, J. M. Feng, B. R. Ma, J. Wang, and L. Q. Kong, 2018: Modeling the warming impact of urban land expansion on hot weather using the Weather Research and Forecasting Model: A case study of Beijing, China. *Adv. Atmos. Sci.*, **35**(6), 723–736, https://doi.org/10.1007/s00376-017-7137-8.

Loikith, P. C., and A. J. Broccoli, 2012: Characteristics of observed atmospheric circulation patterns associated with temperature extremes over North America. *J. Climate*, **25**(20), 7266–7281, https://doi.org/10.1175/JCLI-D-11-00709.1.

Lu, B., J. S. Sun, J. Q. Zhong, Z. W. Wang, and S. Y. Fan, 2017: Analysis of characteristic bias in diurnal precipitation variation forecasts and possible reasons in a regional forecast system over Beijing area. *Acta Meteorologica Sinica*, **75**(2), 248–259, https://doi.org/10.11676/qxxb2017.021. (in Chinese)

Qian, T. T., Y. C. Wang, Z. F. Zheng, and Y. G. Zheng, 2005: A case study of the structure of the Hetao High which caused long-lasting hot weather in Beijing. *Journal of Applied Meteorological Science*, **16**(2), 167–173, https://doi.org/10.3969/j.issn.1001-7313.2005.02.005. (in Chinese)

Takane, Y., and H. Kusaka, 2011: Formation mechanisms of the extreme high surface air temperature of 40.9°C observed in the Tokyo metropolitan area: Considerations of dynamic foehn and foehnlike wind. *J. Appl. Meteor. Climatol*, **50**(9), 1827–1841, https://doi.org/https://doi.org/10.1175/JAMC-D-10-05032.1.

Wang, P. Y., J. P. Tang, X. G. Sun, S. Y. Wang, J. Wu, X. N. Dong, and J. Fang, 2017: Heat waves in China: Definitions, leading patterns, and connections to large-scale atmospheric circulation and SSTs. *J. Geophys. Res.*, **122**(20), 10 679–10 699, https://doi.org/10.1002/2017jd027180.

Wei, J., and J. H. Sun, 2007: The analysis of summer heat wave and sultry weather in North China. *Climatic and Environmental Research*, **12**(3), 453–463, https://doi.org/10.3969/j.issn.1006-9585.2007.03.025. (in Chinese)

Wei, J., H. Yang, and S. Q. Sun, 2004: Relationship between the anomaly longitudinal position of subtropical high in the western Pacific and severe hot weather in North China in summer. *Acta Meteorologica Sinica*, **62**(3), 308–316, https://doi.org/10.11676/qxxb2004.031. (in Chinese)

Wei, K., and W. Chen, 2009: Climatology and trends of high temperature extremes across China in summer. *Atmos. Oceanic Sci. Lett.*, **2**(3), 153–158, https://doi.org/10.1080/16742834.2009.11446795.

Wu, L. Y., J. Y. Zhang, and W. J. Dong, 2011: Vegetation effects on mean daily maximum and minimum surface air temperatures over China. *Chinese Science Bulletin*, **56**(9), 900–905, https://doi.org/10.1007/s11434-011-4349-7.

Zhang, D. K., H. D. Yao, X. W. Yang, and Y. M. Liao, 2006: The regional average method of yearly high temperature day series in North China and its tendency analysis. *Plateau Meteorology*, **25**(4), 750–753, https://doi.org/10.3321/j.issn:1000-0534.2006.04.026. (in Chinese)

Zhang, J., Z. Y. Liu, and L. Chen, 2015: Reduced soil moisture contributes to more intense and more frequent heat waves in northern China. *Adv. Atmos. Sci.*, **32**(9), 1197–1207, https://doi.org/10.1007/s00376-014-4175-3.

Zhang, S. Y., Y. L. Song, D. K. Zhang, and S. R. Wang, 2004: The climatic characteristics of high temperature and the assessment method in the large cities of northern China. *Acta Geographica Sinica*, **59**(3), 383–390, https://doi.org/10.11821/xb200403008. (in Chinese)

Zheng, Z. F., and Y. C. Wang, 2005: A composite analysis of severe heat wave events in Beijing. *Meteorological Monthly*, **31**, 16–20. (in Chinese)

Zhu, J. S., F. Y. Kong, X. M. Hu, Y. Guo, L. K. Ran, and H. C. Lei, 2018: Impact of soil moisture uncertainty on summertime short-range ensemble forecasts. *Adv. Atmos. Sci.*, **35**(7), 839–852, https://doi.org/10.1007/s00376-017-7107-1.